

Full Length Research Paper

High pressure phase stability, elastic anisotropy and electronic properties of BC₂N

Habanyama A.^{1*}, Samukonga G.^{1,2} and Mumba N. K.¹

¹Department of Physics, Copperbelt University, P. O. Box 21692, Jambo Drive, Riverside, Kitwe 10101, Zambia.

²Department of Physics, Mukuba University, P. O. Box 20382, Itimpi, Garnerton, Kitwe 10101, Zambia.

Received 11 December, 2020; Accepted 19 October, 2021

Crystal lattice structure searching by Particle Swarm Optimization (PSO) and first-principles structural optimization have been used to explore polymorphs of BC₂N, possessing sp³ hybridization, under a varying applied hydrostatic pressure. Two low Gibbs free energy structures were identified: one with a primitive orthorhombic structure and Space Group, Pmm2, and the other with a primitive tetragonal structure and Space Group, P m2. Dynamical and mechanical stabilities of the Pmm2, orthorhombic BC₂N (o-BC₂N) structure were established using its phonon dispersions and elastic constants. The bulk modulus of this predicted BC₂N phase was 377.15 GPa, which indicates a super-hard compound. The material is brittle with a B/G ratio of 0.911 and a low degree of elastic anisotropy with a Universal Elastic Anisotropy Index of only 0.774%. Calculations of the electronic band structure demonstrated that the material is a direct band gap semiconductor with a band gap of 1.731 eV at zero applied pressure. The band gap increases monotonically with increased applied pressure and saturates to a value of about 1.756 eV above 1500 kbars; the hydrostatic pressure coefficients associated with this process were determined.

Key words: High pressure phase stability, elastic anisotropy, ultra-hard material.

INTRODUCTION

The strength of super- or ultra-hard materials makes them important for a variety of applications such as, drilling, cutting, wear-resistant coating and abrasives. Diamond is not suitable for machining alloys of iron like steel because, although it is extremely hard, it reacts with iron in the presence of oxygen when the temperature exceeds 80 K (John et al., 2002). An ultra-hard material which is more suitable than diamond for machining ferrous materials is cubic boron nitride (c-BN), because it

is more chemically inert to redox reactions with iron at high temperatures. However, the hardness of c-BN is in the range of only half that of diamond (Singh, 1986). Ternary compounds of the boron-carbon-nitride (B-C-N) system like BC₂N have attracted extensive researcher interest in the search for materials that are harder than c-BN and chemically more stable than diamond at elevated temperatures.

The synthesis of novel super-hard materials is an

*Corresponding author. E-mail: adrian.habanyama@cbu.ac.zm or ahabanyama@yahoo.com Tel: +260 963313923. Fax: +260-212-222881.

important area of frontier research in high-temperature and high-pressure (HTHP) technology. Single crystal super-hard materials have been experimentally synthesized under high temperature and pressure conditions using laser heated diamond-anvil cells (DAC) (Stavrou et al., 2016). There are contradictory results reported by different authors (Nakano, 1996; Kagi et al., 1996) on the attempted experimental synthesis of B–C–N compounds. There is no clarity on whether the resulting materials were solid solutions of carbon with cubic boron nitride or mixtures of dispersed diamond with cubic boron nitride. Nano-crystalline BC₂N has been synthesized by HTHP (Solozhenko et al., 2001; Zhao et al., 2002) and the measured hardness reached 76 GPa (Solozhenko et al., 2001) and 62 GPa (Zhao et al., 2002), which are higher than that for c-BN. It remains a major challenge to determine the crystal structure of BC₂N using experimental methods like x-ray diffraction (XRD) because of the very close and low values of atomic masses for boron, carbon and nitrogen atoms, which are 10.81, 12.01 and 14.01 respectively; these three elements are ‘neighbors’ on the periodic table and their diffraction peaks tend to overlap. Therefore, first principles methods are important in determining the crystal structure of BC₂N polymorphs. This knowledge could assist in developing cheaper methods of synthesizing the material. First principles methods may also assist in exploring other technologically useful properties of BC₂N.

Previous theoretical studies on this material were based on the assumption that BC₂N is a derivative of carbon and boron nitride (BN) structures. These studies therefore proposed phases that are probable derivative combinations of carbon (diamond or graphite) and boron nitride structures like, cubic-BC₂N (Luo et al., 2007^b), zinc blende-BC₂N (Sun et al., 2001) and wurtzite-BC₂N (Luo et al., 2007^a). Some theoretical work on diamond-like boron carbon nitrides (d-BC_xN) (He et al., 2019; Gao et al., 2017, 2018) has also been carried out. In the present study, we have taken an approach using an algorithm called Particle Swarm Optimization or PSO (Gao et al., 2010; Wang et al., 2012) which does not make any initial assumption regarding any starting or derivative structures.

PSO is one of several popular Swarm Intelligence (SI) algorithms. Swarm Intelligence is a part of Artificial Intelligence (AI). In this case, the word “swarm” can be understood in the context of the choreography of a flock of birds, which are a collection of individual elements that perform random iterations. Although these individual elements of a swarm are not centrally controlled, they have memory and can monitor their best past positions, P_{best} (e.g. at energy minima) and their interactive “wellness”, in relation to other members of their population and the environment, at these best positions. Each element can therefore use its memory of past experiences to adjust its direction of motion and speed. After a while the whole swarm converges to a stable

formation. Swarm Intelligence involves the collective study of the individuals’ behavior in population interaction. By considering chemical elements as the individuals of a swarm, we use PSO and swarm convergence in order to predict the formation of compounds of these elements in various atomic bonding environments (e.g., metallic, ionic and covalent bonding).

Atomic binding in ultra-hard materials is predominantly covalent in nature. Plastic and elastic deformations are strongly resisted by covalently bonded materials (Zhao et al., 2016). Ultra-hard materials are often formed by light elements like C, B, O and N (Habanyama et al., 2018) which are suitable for the formation of short directional and shear resistant covalent networks (Hu et al., 2016, 2017).

The electronic properties of B-C-N compounds are also of interest. B, C, and N have 3, 4, and 5 valence electrons, that is, with $2s^22p^1$, $2s^22p^2$ and $2s^22p^3$ as valence electronic configurations respectively. Compound phases of the type, B_xC_yN_z (where, $x = z$) are isoelectronic, that is, they have similar atomic connectivity with the same number of valence electrons. Compounds with this stoichiometry, like BC₂N and BC₄N are expected to be insulators or semiconductors (Zhao et al., 2002; He et al., 2004). In crystals that are mostly covalently bonded, the length and density of the bonds determine the hardness. Partial metallic and a degree of ionic bonding, that is, metallicity (Guo et al., 2008) and iconicity (Gao et al., 2003) respectively, may also have an effect on the hardness. These bonding parameters can be calculated using first principles. Vickers hardness, H_V in GPa can be expressed using a microscopic model of hardness (Guo et al., 2007, 2008) as:

$$H_V (GPa) = 1051 N_e^{\frac{2}{3}} d^{-2.5} \exp(-1.191 f_i - 32.2 f_m^{0.55}) \quad (1)$$

where, N_e is the density of valence electrons associated with the bonds expressed in Å³ units, d is the length of the bonds expressed in angstroms, f_i is the iconicity (Gao et al., 2003; He et al., 2005) in the bonding mechanism and f_m is a factor which expresses the level of metallicity (Guo et al., 2007) in the bonding. The term, $\exp(-1.191 f_i - 32.2 f_m^{0.55})$ in Equation (1) is therefore a correctional factor to account for partial ionic and metallic bonding.

Super-hard materials have a Vickers hardness which is greater than 40 GPa (Solozhenko and Gregoryanz, 2005). The degree of hardness of a material can be estimated or scaled using its shear and bulk moduli (Clerc, 1999). In particular, materials with a bulk modulus greater than 250 GPa are expected to be super-hard (Lowther, 2000). The elastic moduli of essentially all known single crystals depend, to some extent, on the crystals’ orientation. This means that the crystals are anisotropic as opposed to isotropic in their elastic response. An understanding of the susceptibility of a

material to lattice distortions and micro-cracks is very important for its application and this is related to the degree of elastic anisotropy of the material. The effects of anisotropy in several crystal phenomena like phase transformation and dislocation dynamics have been reported (Ledbetter and Migliori, 2006). The present study investigates the compound phases of BC₂N in terms of their stability under a varying hydrostatic pressure, as well as the anisotropic and electronic properties.

COMPUTATIONAL METHODS

The Particle Swarm Optimization (PSO) algorithm (Gao et al., 2010; Wang et al., 2012), which was described earlier was used in a study conducted to determine the structural phases of BC₂N, with the lowest values of the Gibbs free energy, at a temperature of 0K. We made use of the Crystal structure AnaLYsis by Particle Swarm Optimization (CALYPSO) software (Wang et al., 2010) implementation of the PSO algorithm (Gao et al., 2010; Wang et al., 2012). The PSO algorithm tends to achieve swarm convergence prematurely because the best past positions, P_{best} , described in our Introduction, are not controlled by any parameter. In order to avoid this, CALYPSO incorporates additional methods like structural generation symmetry constraints (Wang et al., 2012). The main input to a CALYPSO calculation is the chemical formula (stoichiometry) of the compound to be studied. Several structural phases are generated by the CALYPSO software and displayed according to the magnitude of their enthalpies. Information regarding the space groups of the structures is also generated and displayed. In this study, we investigate two of these structures. Some recent research works (Habanyama and Samukonga, 2021; Gao et al., 2019; Wang et al., 2019; Su et al., 2017) has successfully made use of the CALYPSO software package.

In the present work, Particle Swarm Optimization simulations were performed where a unit cell had up to 16 atoms. Quantum Espresso (Giannozzi et al., 2009), which is a widely used implementation of the Density Functional Theory (DFT), was used to perform the PSO associated structural optimization procedures. Some structural and electronic properties were also determined using Quantum Espresso simulations. The interaction between electrons and ion cores were modeled using the Andrea Dal Corso-type ultra-soft pseudo-potentials (USPP) for N, B and C with the respective valence electronic configurations, $2s^22p^3$, $2s^22p^2$ and $2s^22p^1$. The exchange interaction and correlation between electrons was calculated using the Generalized Gradient Approximation (GGA-PBE) model (Perdew et al., 1996). The plane-wave functions' cut-off kinetic energy used was 70 Ry and the k-point mesh was sampled as $16 \times 16 \times 16$ Monkhorst Pack (Monkhorst and Pack, 1976) in the Brillouin zone. The threshold of the self-consistent field (SCF) was convergent within 10^{-3} eV/atom. The Xcrystden software package (Kokalj, 2003) was used to visualize the predicted crystal structures. The structures were then tested for energetic (thermodynamical), vibrational (dynamical) and elastic (mechanical) stabilities.

Thermodynamical or energetic stability depends on Gibbs free energy, G of the system

$$G = E + PV - TS \quad (2)$$

A structural phase with the lowest value of G is the most thermodynamically stable phase, where S is the entropy of the system, T is the temperature, P is the pressure, volume is V and the internal energy is E . If the pressure on a stable structural phase is

increased, its Gibbs free energy can become equal to that of another phase. If a further increase in pressure causes the phase with the previously lower Gibbs free energy to have a higher energy than the other phase, then a pressure induced phase transformation occurs. It is assumed in our calculations that the structures of the compounds being studied are in their ground states at absolute zero of temperature. We calculate the enthalpy, H as a function of pressure in order to predict any possible structural phase transitions,

$$H = E + PV \quad (3)$$

The pressure at absolute zero of temperature is given by

$$P = -\frac{\partial E}{\partial V} \quad (4)$$

The transition pressure can therefore be determined by computing the variation of the internal energy at different volumes of the unit-cell.

In order to establish the vibrational or dynamical stability of a material, the entire spectrum of its lattice vibrational modes needs to be analyzed. For a material to be dynamically stable, all lattice frequency calculations at reciprocal lattice vectors in the Brillouin zone should be positive, since negative values would imply imaginary or non-existent phonons. We used two different methods to calculate phonon dispersion frequencies and spectra. In the first method, we only performed phonon calculations at the Brillouin zone center (the Γ point). In this case, we used the density functional perturbation or "linear response" theory (Baroni et al., 1987; Giannozzi et al., 1991) as implemented by the Quantum Espresso package. The second method used was the finite displacement and supercell method, as implemented by the Phonopy (Togo and Tanaka, 2015) software package. We performed calculations along \mathbf{k} -point paths such that the resulting phonon dispersion curves covered the Brillouin zone. In these calculations, controlled forces are induced on the atoms by systematically displacing them from their equilibrium positions and storing this displacement information in supercells. Our BC₂N calculations used $2 \times 2 \times 2$ supercells with 64 atoms. The induced atomic forces were calculated from each supercell using Quantum Espresso. The Phonopy package was then used to extract the atomic displacement information together with the corresponding induced atomic forces in order to generate force constants and build dynamic matrices. The dynamic matrices were used to calculate phonon frequencies along the required \mathbf{k} -point paths. In both the density functional perturbation theory application and the finite displacement and supercell method, the units of the frequencies presented in the results were, THz (4 meV \sim 1 THz).

Second order elastic constants need to be considered in order to establish the elastic or mechanical stability of a material. The bulk and shear moduli were determined using three different methods. The first method assumes a uniform strain, also known as the Voigt calculation (Voigt, 1928). The second method assumes uniform stress, this is the Reuss (Reuss and Angew, 1929) calculation and thirdly the averaging of the Voigt and Reuss calculations gives the Hill (Hill, 1963) values.

To obtain the Voigt bulk and shear moduli, represented as B_V and G_V respectively, Equations (5) and (6) were used:

$$B_V = (1/9)[(C_{33} + C_{22} + C_{11}) + 2(C_{23} + C_{13} + C_{12})] \quad (5)$$

and

$$G_V = (1/15)[(C_{33} + C_{22} + C_{11}) - (C_{23} + C_{13} + C_{12}) + 3(C_{66} + C_{55} + C_{44})], \quad (6)$$

C_{ij} being the stiffness constants.

To calculate the Reuss bulk and shear moduli, represented as B_R and G_R respectively, we used Equations (7) and (8):

$$B_R = 1/[(S_{33} + S_{22} + S_{11}) + 2(S_{23} + S_{13} + S_{12})] \quad (7)$$

and

$$G_R = 15/[4(S_{33} + S_{22} + S_{11}) - (S_{23} + S_{13} + S_{12}) - 3(S_{66} + S_{55} + S_{44})] \quad (8)$$

S_{ij} being the compliances.

Equations (9) and (10) were used to obtain the averages or Hill values of the shear and bulk moduli respectively:

$$G_H = \frac{1}{2}(G_V + G_R) \quad (9)$$

and

$$B_H = \frac{1}{2}(B_V + B_R). \quad (10)$$

Equations (11) and (12) were used to obtain Hill averages of the Young modulus, E_H and Poisson's ratio, ν_H :

$$E_H = \frac{9B_H G_H}{3B_H + G_H} \quad (11)$$

and

$$\nu_H = \frac{3B_H - 2G_H}{2(3B_H + G_H)}, \quad (12)$$

respectively. Unless indicated otherwise, all results of the elastic moduli presented in this work are Hill values.

Cubic crystals exhibit elastic isotropy in terms of their bulk modulus alone and $B_V = B_R$. Any anisotropy in a cubic lattice is purely shear related where, $G_V \neq G_R$. In lattice structures that are not cubic, both shear and bulk moduli anisotropies are present. The Universal Elastic Anisotropy Index, A_U (Ranganathan and Ostoja-Starzewski, 2008),

$$A_U = 5 \frac{G_V}{G_R} + \frac{B_V}{B_R} - 6 \quad (13)$$

gives a way of quantifying the combined degree of anisotropy due to both shear and bulk moduli. We see from Equation (13) that when a crystal is totally isotropic then, $G_V = G_R$ and $B_V = B_R$; therefore, $A_U = 0$. It is the degree of departure from zero of the Universal Elastic Anisotropy Index that quantifies the level of elastic anisotropy in a crystalline material.

RESULTS

Two low Gibbs free energy crystal structures were identified in our search to determine the polymorphs of BC_2N . The first structure had the Hermann Mauguin Space Group, Pmm2 [space group number index, 25]. This is an orthorhombic Bravais lattice with the Point Group, mm2. It has a primitive lattice type as signified by the 'P' in the space group. The second structure had the Hermann Mauguin Space Group, $P\bar{4}m2$ [space group number index, 115]. This is a primitive tetragonal Bravais lattice with the Point Group, $\bar{4}2m$. Figures 1(a) and (b)

show diagrams of these two structures as visualized by the Xcrysden software package (Kokalj, 2003).

There are no boron-to-boron (B-B) bonds seen in Figures 1(a) and (b). According to previous studies (Sun et al., 2001; Nozaki and Itoh, 1996), B-B bonds are not expected to exist in covalently bonded structures of the B-C-N system because they would make the structures less stable by effectively increasing the total energy of the system.

Total-energy calculations were used to analyze the response of the two BC_2N structural phases in Figures 1(a) and (b) under hydrostatic compression. We started these calculations with an equilibrium lattice parameter at absolute zero of temperature; thereafter the pressure was increased incrementally. At each fixed value of the pressure, the unit-cell volume, the internal energy and the enthalpy, H were calculated. Figure 2 is a graphic presentation of the changes in enthalpies for the two structures with increased hydrostatic pressure in the range from 0 to 1400 kbar.

The orthorhombic, Pmm2 structure is seen to be more thermodynamically stable than the tetragonal, $P\bar{4}m2$ structure in the entire pressure range. The fact that the two graphs do not cross each other means that a pressure-induced phase transition is not possible between these two structures within the pressure range investigated.

Figure 3(a) shows a plot of the internal energy against the volume of the BC_2N unit cell. Figure 3(b) shows a similar plot for germanium, which demonstrates the so-called, "common tangent" construction. The transition pressure between the two Ge phases in Figure 3(b) is the negative of the common tangent's gradient. The study of Ge is not part of the current work but Figure 3(b) was included for the sole purpose of comparing it to Figure 3(a), hence demonstrating that there is no possible common tangent between the energy-against-volume plots of the BC_2N phases and therefore no possible phase change.

Table 1 presents our BC_2N phonon calculation results under zero pressure at the Brillouin zone center (the Γ point). The tetragonal structure exhibits some negative frequencies as seen in the table, indicating that it is not dynamically stable. On the other hand, the orthorhombic phase could possibly be stable as no negative phonon frequencies are seen for the Γ point. The orthorhombic structure was therefore subjected to further tests while no further work was carried out on the tetragonal structure.

Some high symmetry points and lines are shown in the first Brillouin zone of the primitive lattice of the orthorhombic structure in Figure 4.

The finite displacement and supercell method, as implemented by the Phonopy software package (Togo and Tanaka, 2015) was used to perform phonon calculations for the orthorhombic BC_2N along the k -point path: $\Gamma \rightarrow R \rightarrow Z \rightarrow T \rightarrow Y \rightarrow S \rightarrow \Gamma \rightarrow X$. Figure 5 shows the resulting phonon dispersion curves.

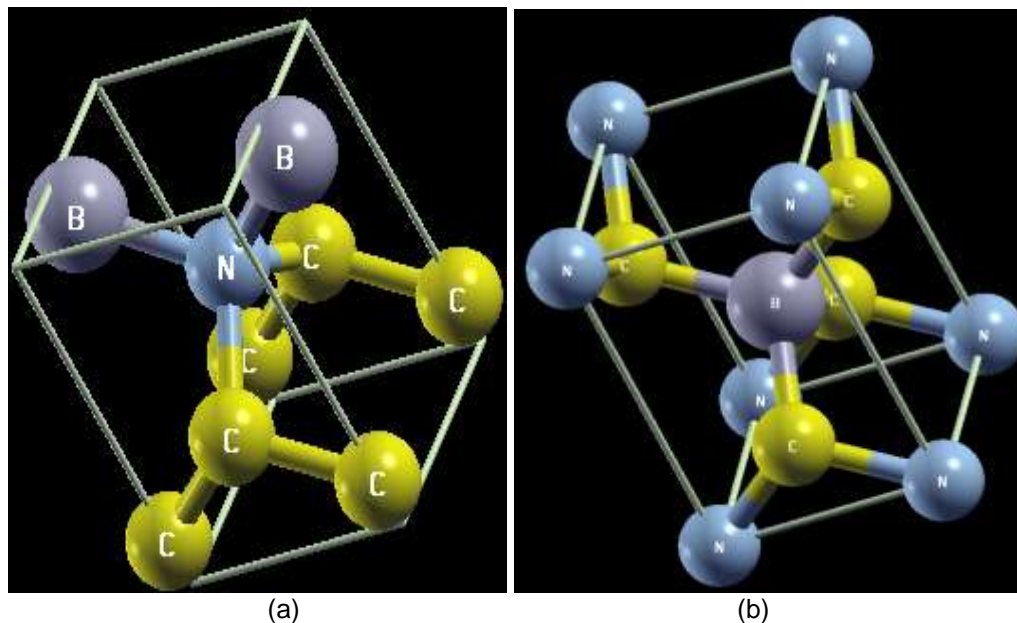


Figure 1. (a) An Orthorhombic BC_2N lattice cell having Hermann Mauguin Space Group, $Pmm2$ [SG index, 25] and Point, Group, $mm2$. (b) A Tetragonal BC_2N lattice cell having Hermann Mauguin Space Group, $P\bar{4}m2$ [SG index, 115] and Point Group, $\bar{4}2m$.

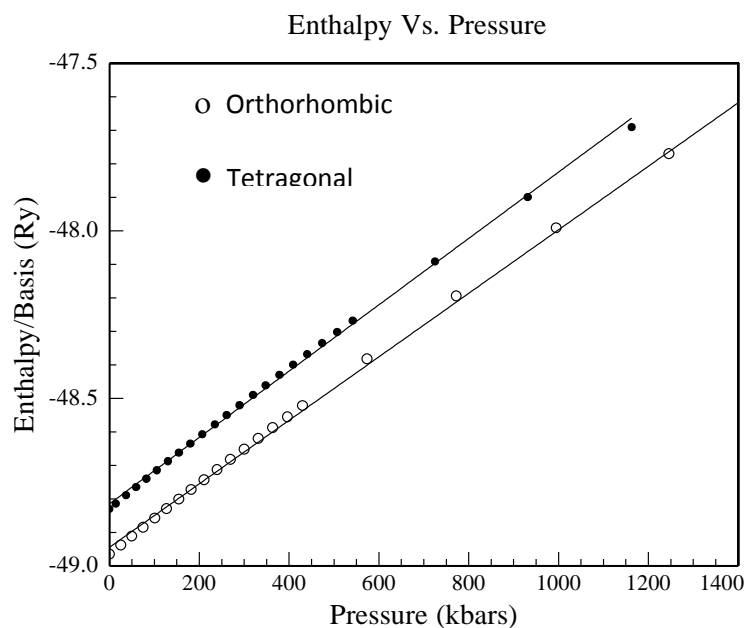


Figure 2. Enthalpies per four atom formula unit of tetragonal BC_2N (solid circles) and orthorhombic BC_2N (open circles) plotted against the hydrostatic pressure.

Table 1 shows that the lowest and highest phonon frequencies are 3.3164 and 37.7817 THz respectively. Figure 5 shows the natural vibrational frequencies of orthorhombic BC_2N to be in a band from about 0.0 to 38

THz. Our finite displacement and supercell method results are therefore in general agreement with our density functional perturbation theory results. The absence of negative phonon frequencies throughout the

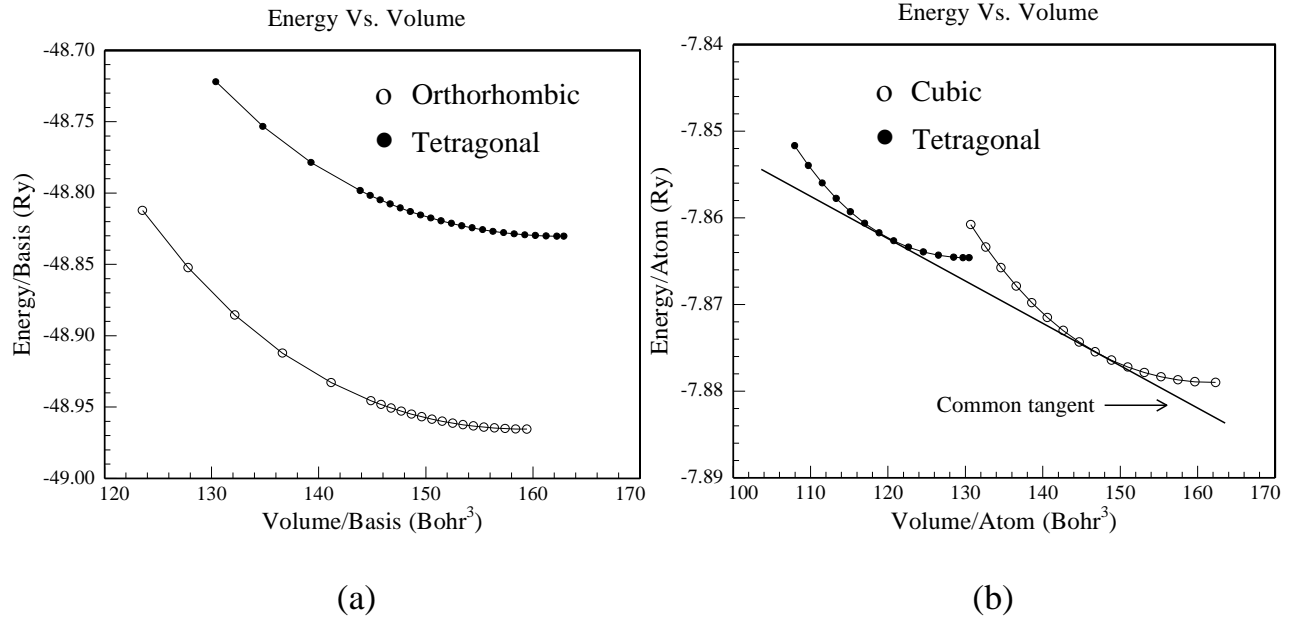


Figure 3. (a) Plots of the total energy against the volume per four atom formula unit of tetragonal BC₂N (solid circles) and orthorhombic BC₂N (open circles). (b) Plots of the total energy against the volume per atom of beta-tin (tetragonal) Ge (solid circles) and zinc-blende (cubic-diamond) Ge (open circles).

Table 1. A table giving phonon results calculated at the Brillouin zone centers (Γ points).

Crystal structure and space group	Orthorhombic Space Group, Pmm2 [SG index, 25]		Tetragonal Space Group, P $\bar{4}$ m2 [SG index, 115]	
	THz	cm ⁻¹	THz	cm ⁻¹
1	3.3164	110.6	-4.3096	-143.8
2	4.1544	138.6	-3.1906	-106.4
3	4.1544	138.6	1.5641	52.2
4	20.7874	693.4	20.8932	696.9
5	20.7874	693.4	21.0983	703.8
6	23.0547	769.0	22.4309	748.2
7	23.0547	769.0	27.2039	907.4
8	31.6981	1057.3	30.5513	1019.1
9	32.1565	1072.6	33.9803	1133.5
10	35.5218	1184.9	36.1939	1207.3
11	37.7817	1260.3	37.1413	1238.9
12	37.7817	1260.3	37.8533	1262.7

Brillouin zone of the orthorhombic BC₂N lattice structure indicates that it is dynamically stable.

Since the orthorhombic structure was identified as being dynamically stable, it was further tested for mechanical stability. Table 2 shows the Elastic package (Golesorkhtabar et al., 2013) calculation results of the elastic stiffness and compliance constants. This structure had the lattice parameters, $a = 4.791$ Bohr, $b/a = 1.011$ and $c/a = 1.436$. No hydrostatic pressure was applied

during the determination of the elastic stiffness and compliance constants in Table 2.

Table 3 presents the eigenvalues of the stiffness matrix obtained by diagonalization using the Eigen (Guennebaud and Jacob, 2010) C++ template library for linear algebra. The Reuss and Voigt shear and bulk moduli are presented in Table 4. The value of the Universal Elastic Anisotropy Index, which was calculated using Equation (13), is also presented.

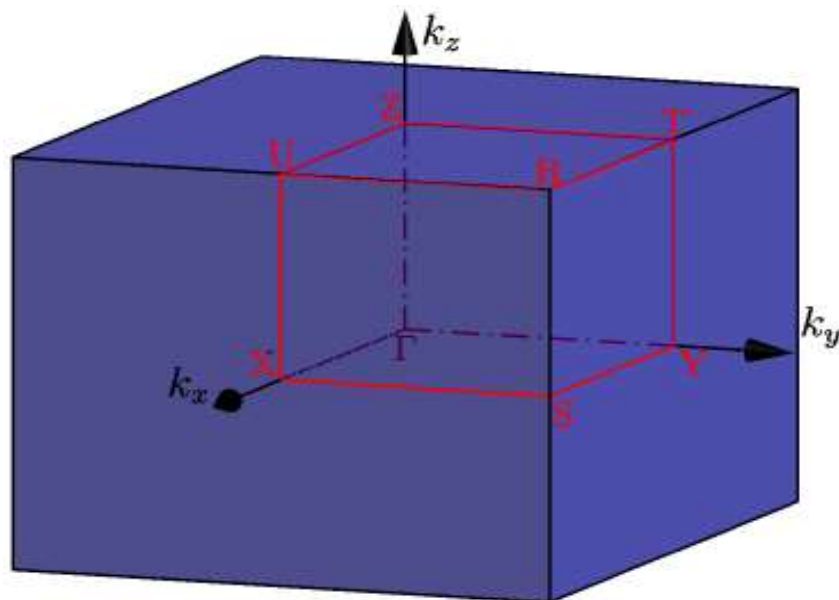


Figure 4. High symmetry points and lines of the simple orthorhombic Brillouin zone.

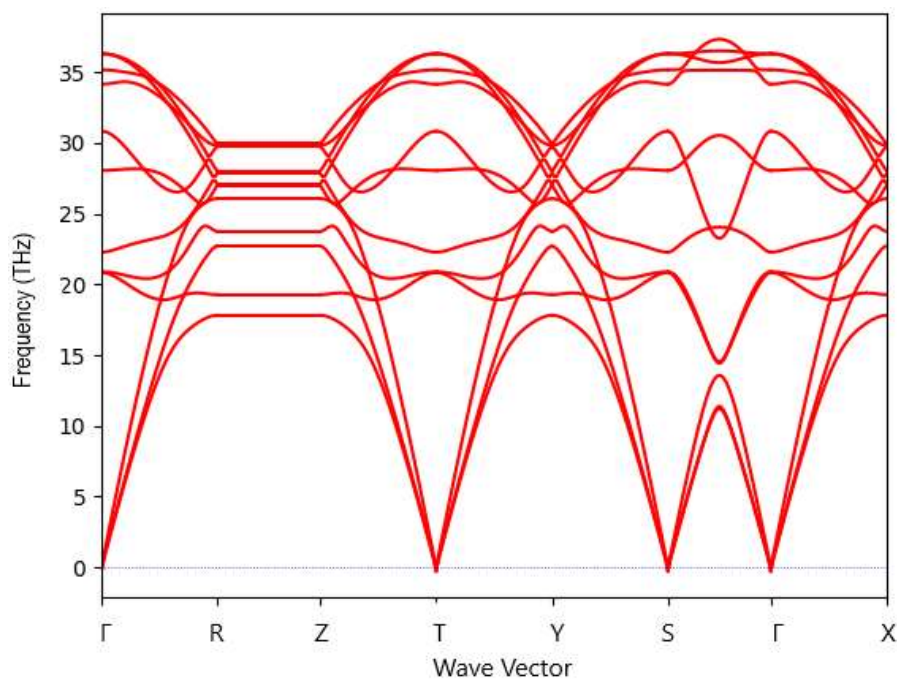


Figure 5. Dispersion curves for orthorhombic BC₂N, with phonon frequencies calculated using the Phonopy software package.

Table 5 presents the Elastic package (Golesorkhtabar et al., 2013) calculated Hill values of the bulk, shear and Young moduli, for orthorhombic BC₂N (*o*-BC₂N). The values of the Poisson's and *B/G* ratios are also shown.

In order to study some electronic properties of *o*-BC₂N, its electronic energy band structure was calculated along

the *k*-point path, $\Gamma \rightarrow R \rightarrow Z \rightarrow T \rightarrow Y \rightarrow S \rightarrow \Gamma \rightarrow X$. The high symmetry points and lines in the first Brillouin zone are as shown in Figure 4. The resulting energy band diagram, under zero hydrostatic applied pressure is shown in Figure 6. It should be made clear that the actual computed energy of the Fermi level, E_F was 13.9497 eV.

Table 2. The only non-zero independent second order elastic constants for orthorhombic BC₂N

Stiffness matrix elements, C_{ij} (GPa) and compliances, S_{ij} ($\times 10^{-5}$ GPa ⁻¹)								
C_{11}	C_{12}	C_{13}	C_{22}	C_{23}	C_{33}	C_{44}	C_{55}	C_{66}
S_{11}	S_{12}	S_{13}	S_{22}	S_{23}	S_{33}	S_{44}	S_{55}	S_{66}
1031.7	20	141.1	908.2	131.8	873.5	401.4	475.5	367.5
99	0.4	-16	113	-17	120	249	210	272

Table 3. Resultant eigenvalues from the diagonalization of the stiffness matrix for orthorhombic BC₂N.

S/N	Stiffness matrix, C_{ij} (GPa) eigenvalues
1	1147.9
2	939.9
3	725.6
4	401.4
5	475.5
6	367.5

Table 4. Computed Shear and bulk moduli for orthorhombic BC₂N using the Reuss and Voigt methods along with presentation of the Universal Elastic Anisotropy Index.

B_V (GPa)	B_R (GPa)	G_V (GPa)	G_R (GPa)	Universal Elastic Anisotropy Index, A_U	Percentage Anisotropy
377.70	376.61	416.92	410.79	0.0774	0.774%

Table 5. Orthorhombic BC₂N averaged Hill values of the shear, bulk and Young moduli presented together with the B/G and Poisson's ratios.

Bulk Modulus B (GPa)	Shear Modulus G (GPa)	Young Modulus E (GPa)	B/G	Poisson's Ratio, ν
377.15	413.86	909.06	0.911	0.10

The energy axis in Figure 6 was shifted upwards by 13.9497 eV so as to place the Fermi level at the origin ($E = 0$).

It was determined from the calculations that the material has an energy band gap of 1.731 eV when there is no applied hydrostatic pressure. This is a direct band gap as seen in Figure 6. The width of the band gap suggests that this is a semiconductor because semiconductors generally have a band gap energy, $E_g \leq 3.0$ eV.

In Figure 7(a), the energy of the 'bottom' edge of the conduction band, which is the lowest unoccupied energy level at temperature, $T = 0$, is plotted together with the energy of the 'top' edge of the valence band, which is the maximum occupied energy level at, $T = 0$, as a function of the applied pressure.

As pointed out earlier, the origin of the energy axis in Figure 6 is placed at the Fermi level, E_F however, in Figure 7(a) the origin is placed such that the Fermi level at zero pressure is at its actual computed value of

13.9497 eV. The lowest energy level of the conduction band at zero pressure, $P = 0$ kbars, is 14.8152 eV and the highest level in the valence band at zero pressure is, 13.0842 eV, giving an energy band gap of 1.731 eV, at $P = 0$ kbars. The energy difference between the two curves in Figure 7(a) gives the value of the band gap at each value of the applied pressure. Figure 7(b) shows the width of the energy band gap as a function of the applied pressure. Figure 7(b) shows that an increasing applied pressure results in a monotonic increase in the band gap. It is likely that as the applied pressure is increased, a saturation value for the band gap would eventually be arrived at, which is evident from the curvature of the graph.

DISCUSSION

It is seen in Table 3 that the eigenvalues of the stiffness matrix, C_{ij} for orthorhombic BC₂N are all positive. This

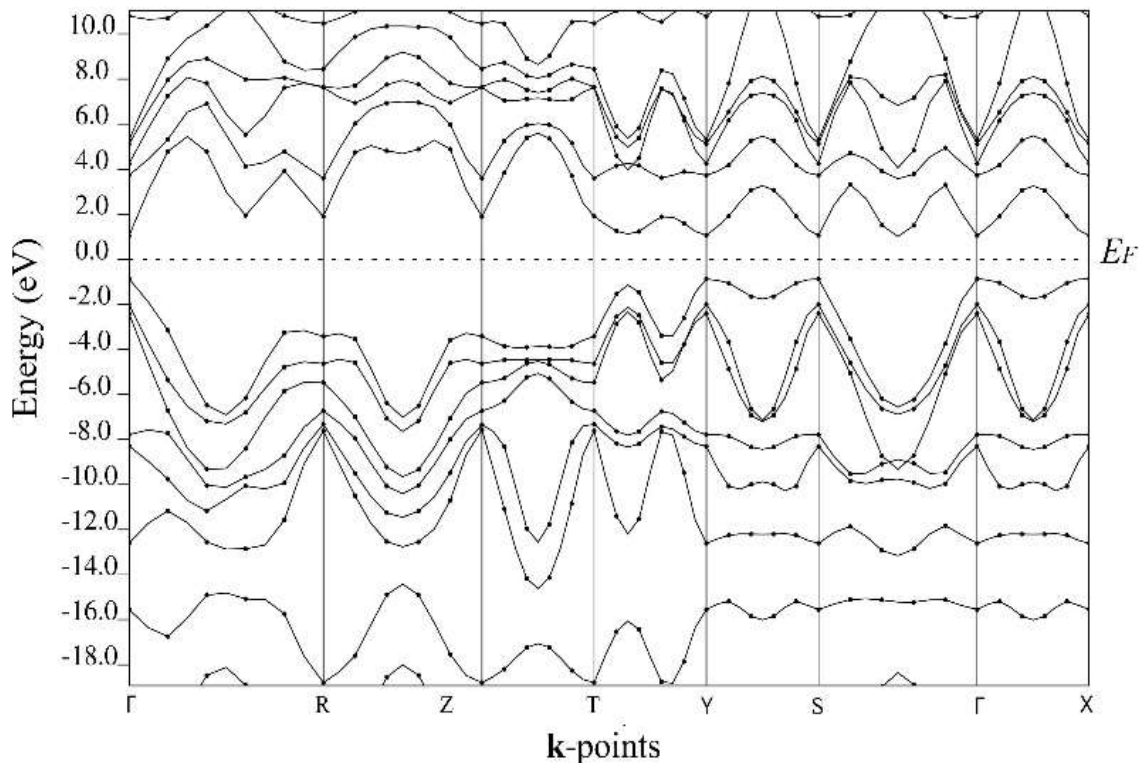


Figure 6. The orthorhombic BC₂N electronic energy band structure, with no applied hydrostatic pressure. The energy axis is shifted upwards by 13.9497 eV so as to place the Fermi level at the origin ($E = 0$).

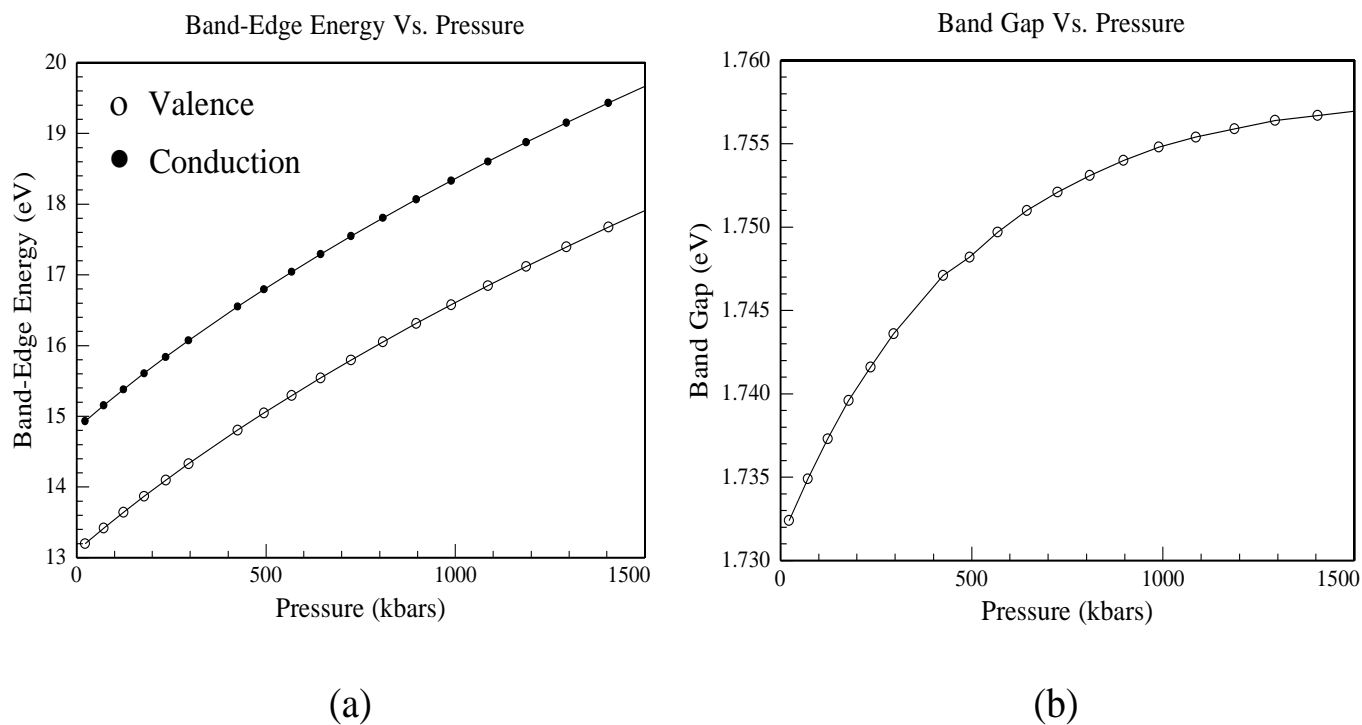


Figure 7. (a) Electronic energy at the bottom of the conduction band at temperature, $T = 0$, plotted together with that at the top of the valence band, against the applied pressure. (b) Graph of the energy band gap of *o*-BC₂N as function of the hydrostatic pressure.

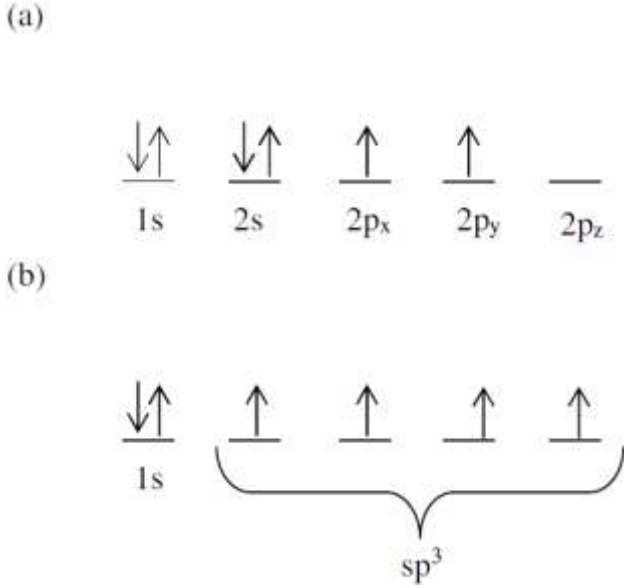


Figure 8. (a) The 1s and 2s electrons are paired with opposite spins but the 2p electrons are unpaired. (b) A 2s electron shifts to the p level forming four hybrid sp^3 orbitals with unpaired electrons.

fulfils the generic condition for mechanical stability. However, a specific and sufficient Born criterion (Born and Huang, 1954) for testing the mechanical stability of an orthorhombic structure was modified by Mouhat and Coudert (2014), as the inequality:

$$C_{11}C_{22}C_{33} + 2C_{12}C_{13}C_{23} - C_{11}C_{23}^2 - C_{22}C_{13}^2 - C_{33}C_{12}^2 > 0 \quad (14)$$

The results in Table 2 satisfy the Inequality (14), indicating that orthorhombic BC_2N is mechanically stable.

The Universal Elastic Anisotropy Index of α - BC_2N is, $A_U = 0.774\%$, as seen in Table 4. This value, which is less than 1%, indicates that the degree of anisotropy of the material is such that its susceptibility to micro-cracks is low. This material is essentially isotropic in response to hydrostatic compression without shearing because its Voigt and Reuss bulk moduli are almost equal, that is, $B_V \approx B_R$. The ratio B/G reflects the brittleness of a material. According to Pugh (1954), the ratio, B/G is greater or equal to the value 1.75 for ductile materials and it is less than 1.75 for brittle materials. Orthorhombic BC_2N is therefore a brittle material with a B/G ratio of 0.911 as seen in Table 5.

Table 5 shows that the value of the Young modulus for α - BC_2N is large. This elastic modulus relates a stress to the resulting strain in the same direction. Poisson's ratio gives an indication of the plasticity of a material. Table 5 presents a low value of the Poisson's ratio, $\nu = 0.10$, which indicates a relatively low level of plasticity. Table 5 also shows that the values of both the bulk and shear

moduli of α - BC_2N are large. Ultra-hard materials are known to have values of the bulk modulus exceeding 250 GPa (Lowther, 2000); hence α - BC_2N is therefore a potentially super-hard material with a bulk modulus of about 377 GPa.

The carbon atoms in B-C-N materials possess sp^3 hybrid orbitals which facilitate the mechanism behind the ultra-hardness of these materials (Luo et al., 2007a, b). Figure 8(a) shows how electrons occupy the orbitals of the carbon atom. The diagram shows that the 1s and 2s electrons are paired with opposite spins but the 2p electrons are unpaired. Figure 8(b) shows the excited carbon atom electronic configuration during the synthesis of super-hard materials, where a 2s electron shifts to the p level forming four energetically similar mixed (hybrid) sp^3 orbitals with electrons that are not paired.

The sp^3 hybrid orbitals bond covalently with B, N and other C atoms in α - BC_2N . These bonds are short, dense and directional, resulting in highly shear resistant 3-dimensional networks. This is the fundamental origin of the super-hardness of α - BC_2N .

The pure hydrostatic strain which is created in high pressure experiments, such as those that use diamond anvil cells (DACs), causes a reduction in the distance between atoms which results in enhanced overlapping between the wave functions of neighboring atoms in a material. The valence electron states in BC_2N are highly hybridized as explained earlier and the overlapping of electron orbitals due to the volume reduction can cause a charge transfer between s, p or d states in both the conduction and valence bands. This interaction between states in the conduction and valence bands causes the energies of the conduction or valence bands to be lowered or increased by unequal shifts at different symmetry points of the Brillouin zone. This results in a net decrease or increase of the band gap width at various values of hydrostatic pressure. Figure 7(b) shows that, in the case of α - BC_2N , we observe a net increase in the width of the band gap as the pressure increases. The variation of the band gap with volume can be expressed in terms of the hydrostatic volume deformation potential, a_g defined as (Dridi et al., 2002; Bouhafs et al., 2000)

$$a_g = \frac{dE_g}{d \ln V}, \quad (15)$$

where, E_g is the band gap energy width and V the volume. This commonly used definition given in Equation (15) is actually a relative deformation potential between the bands involved as opposed to an absolute deformation potential

$$a_i = \frac{dE_i}{d \ln V}, \quad (16)$$

of an energy state E_i . The values for a_g are difficult to

obtain experimentally; only the pressure dependence of the energy gap is usually measured. It is therefore convenient to work with the pressure coefficient, dE_g/dP , which is related to the deformation potential through the bulk modulus, B as (Dridi et al., 2002; Bouhafs et al., 2000)

$$a_g = -B \frac{dE_g}{dP}. \quad (17)$$

This definition of the pressure coefficient is useful when the band gap, E_g varies linearly with the applied pressure. However, in nonlinear cases like that of our graph in Figure 7(b), we can extend the definition of pressure coefficients by fitting the data to an empirical quadratic function (Dridi et al., 2002; Bouhafs et al., 2000)

$$E_g(P) = E_g(0) + \alpha P + \beta P^2, \quad (18)$$

where, $E_g(0)$ is the band gap with no applied hydrostatic pressure, the linear term, $\alpha = dE_g/dP$, is the first-order pressure derivative, while the quadratic term, $\beta = d^2E_g/dP^2$, is the second-order pressure derivative. The derivatives α and β are both hydrostatic pressure coefficients. After fitting the data displayed in Figure 7(b) to the quadratic function in Equation (18), we get $E_g(0) = 1.731$ eV, $\alpha = 3.688 \times 10^{-5}$ eV/kbar = 0.3688 meV/GPa and $\beta = -1.436 \times 10^{-8}$ eV/kbar² = -1.436×10^{-5} meV/GPa².

Conclusion

We studied two polymorphs of BC₂N with low Gibbs free energies. One with a primitive orthorhombic structure and Space Group, Pmm2, and the other with a primitive tetragonal structure and Space Group, P $\bar{4}$ m2. The only polymorph found to be both mechanically and dynamically stable was the orthorhombic BC₂N (*o*-BC₂N). As seen in Table 5, the bulk modulus of this material is much greater than 250 GPa. It is therefore expected to be super-hard (Lowther, 2000). Having a B/G value of 0.911, *o*-BC₂N is a brittle material. It is seen in Table 4 that *o*-BC₂N has a Universal Elastic Anisotropy Index of only 0.774%, meaning that it has a low degree of anisotropy indicating a low susceptibility to micro-cracks. The material has been shown to possess a direct band gap of 1.731 eV at zero applied pressure and is likely to be a semiconductor. The band gap increases monotonically with increased applied pressure and saturates to a value of around 1.756 eV at pressures greater than 1500 kbars. Two hydrostatic pressure coefficients were determined; the first-order pressure derivative α was found to have a value of 0.3688 meV/GPa, while the second-order derivative, β was found to be -1.436×10^{-5} meV/GPa². Orthorhombic BC₂N is

expected to be a more suitable semiconductor for high pressure applications than silicon and germanium because unlike Si and Ge it is not likely to undergo any pressure induced phase transitions, as demonstrated by Figures 2 and 3.

CONFLICT OF INTERESTS

The authors have not declared any conflict of interests.

ACKNOWLEDGEMENTS

The authors gratefully appreciate the institutional support provided by the Mukuba and Copperbelt Universities in terms of computational facilities.

REFERENCES

- Baroni S, Giannozzi P, Testa A (1987). Greens-function approach to linear response in solids Physical Review Letters 58:1861.
- Born M, Huang K (1954). Dynamics Theory of Crystal Lattices, Oxford University Press.
- Bouhafs B, Aourag H, Certier M (2000). Trends in band-gap pressure coefficients in boron compounds BP, BAs and BSb Journal of Physics: Condensed Matter 12:5655.
- Clerc DG (1999). Ab initio elastic properties of diamond-like materials: electronic factors that determine a high bulk modulus Journal of Physics and Chemistry of Solids 60:103.
- Dridi Z, Bouhafs B, Ruterana P (2002). Pressure dependence of energy band gaps for Al_xGa_{1-x}N, In_xGa_{1-x}N and In_xAl_{1-x}N. New Journal of Physics 4(94):1-94.15.
- Gao FM, He JL, Wu ED, Liu SM, Yu DL, Li DC, Zhang SY, Tian YJ (2003). Hardness of Covalent Crystals Physical Review Letters 91:015502.
- Gao Y, Wu Y, Huang Q, Ma M, Pan Y, Xiong M, Li Z, Zhao Z, He J, Yu D (2017). Superhard sp²-sp³ hybridized BC₂N: A 3D crystal with 1D and 2D alternate metallicity Journal of Applied Physics. 121: 225103.
- Gao Y, Wu Y, Huang Q, Ma M, Pan Y, Xiong M, Li Z, Zhao Z, He J, Yu D (2018). First principles studies of superhard BC₂N phases with unexpected 1D metallicity. Computational Materials Science 148:157.
- Gao B, Gao P, Lu S, Lv J, Wang Y, Ma Y (2019). Interface structure prediction via CALYPSO method Science Bulletin 64:301.
- Giannozzi P, de Gironcoli S, Pavone P, Baroni S (1991). Ab initio calculation of phonon dispersions in semiconductors Physical Review B 43:7231.
- Giannozzi P, Baroni S, Bonini N, Calandra M, Car R, Cavazzoni C, Ceresoli D, Chiarotti GI, Cococcioni M, Dabo I, Dal Corso A, de Gironcoli S, Fabris S, Fratesi G, Gebauer R, Gerstmann U, Gougoussis C, Kokalj A, Lazzeri M, Martin-Samos I, Marzari N, Mauri F, Mazzarello R, Paolini S, Pasquarello A, Paulatto I, Sbraccia C, Scandolo S, Sclauzero G, Seitsonen AP, Smogunov A, Umari P, Wentzovitch RM (2009). QUANTUM ESPRESSO: a modular and open-source software project for quantum simulations of materials Journal of Physics: Condensed Matter 21:395502.
- Golesorkhtabar R, Pavone P, Spitaler J, Puschnig P, Draxl C (2013). ElaStic: A tool for calculating second-order elastic constants from first principles Computer Physics Communications 184: 1861.
- Guennebaud G, Jacob B (2010). Eigen v3, <http://eigen.tuxfamily.org/>.
- Guo XJ, Liu ZY, Luo XG, Yu DL, He JL, Tian YJ, Sun J, Wang HT (2007). Theoretical hardness of the cubic BC₂N. Diamond and Related Materials 16:526.
- Guo X, Li L, Liu Z, Yu D, He J, Liu R, Xu B, Tian Y, Wang HT (2008). Hardness of covalent compounds: Roles of metallic component and *d* valence electrons Journal of Applied Physics 104:023503.

- Habanyama A, Msikita M, Simfukwe J, Baliga GT, Mumba NK, Mulenga M, Samukonga G (2018). Study of ultra-hard materials of the B-C-N-O quaternary system. *Results in Physics* 11:984-993.
- Habanyama A, Samukonga G (2021). Electronic properties, high pressure phase stability and elastic anisotropy of BC₅. *Scientific African, Elsevier* 11:e00710.
- He JL, Guo LC, Wu E, Luo XG, Tian YL (2004). First-principles study of B₂CN crystals deduced from the diamond structure *Journal of Physics: Condensed Matter* 16:8131.
- He JL, Wu ED, Wang HT, R. Liu RP, Tian YJ (2005). Ionicities of Boron-Boron Bonds in B₁₂ Icosahedra *Physical Review Letters* 94:015504.
- He XL, Shao X, Chen T, Tai YK, Weng X J, Chen Q, Dong X, Gao G, Sun J, Zhou XF, Tian Y, Wang HT (2019). Predicting three-dimensional icosahedron-based boron B₆₀ *Physical Review B*: 99:184111.
- Hill R (1963). Elastic properties of reinforced solids: some theoretical principles, *Journal of the Mechanics and Physics of Solids* 11:357.
- Hu M, He J, Zhao Z, Strobel TA, Hu W, Yu D, Sun H, Liu L, Li Z, Ma M, Kono Y, Shu J, Mao H, Fei Y, Shen G, Wang Y, Juhl SJ, Huang JY, Liu Z, Xu B, Tian Y (2017). Compressed glassy carbon: An ultrastrong and elastic interpenetrating graphene network *Science Advances* 3:e1603213.
- Hu YJ, Xu SL, Wang H, Liu H, Xu XC, Cai YX (2016). Superhard BC₂N: An orthogonal crystal obtained by transversely compressing (3,0)-CNTs and (3,0)-BNNTs. *Chinese Physics Letters* 33:106102.
- John P, Polwart N, Troupe CE, Wilson JIB (2002). The oxidation of (100) textured diamond *Diamond and Related Materials* 11:861.
- Kagi H, Tsuchida I, Masuda Y, Okuda M, Katsura K, Wakatsuki M (1996). Proceedings of the Fifteenth AIRAPT International Conference edited by Trzeciakowski WA ~World Scientific, Singapore pp. 258-260.
- Kokalj A (2003). Computer graphics and graphical user interfaces as tools in simulations of matter at the atomic scale *Computational Materials Science* 28:155.
- Ledbetter H, Migliori A (2006). A general elastic-anisotropy measure *Journal of Applied Physics*. 100: 063516.
- Li P, Gao G, Wang Y, Ma Y (2010). Crystal Structures and Exotic Behavior of Magnesium under Pressure *Journal of Physical Chemistry* 114:21745.
- Lowther JE (2000). Superhard materials. *Physica Status Solidi*, (b). 217(1), 533-543.
- Luo X, Guo X, Liu Z, He J, Yu D, Xu B, Tian Y, Wang H (2007a). First-principles study of wurtzite BC₂N *Physical Review B* 76: 092107.
- Luo X, Guo X, Xu B, Wu Q, Hu Q, Liu Z, He J, Yu D, Tian Y, Wang H (2007b). Body-centered superhard BC₂N phases from first principles. *Physical Review B* 76:094103.
- Monkhorst HJ, Pack JD (1976). Special points for Brillouin-zone integrations *Physical Review B*. 13: 5188.
- Mouhat F, Coudert FX (2014). Necessary and sufficient elastic stability conditions in various crystal systems *Physical Review B* 90:224104.
- Nakano S (1996). Proceedings of the NIRIM International Symposium on Advanced Materials ~NIRIM, Tsukuba, Japan pp. 287-292.
- Nassau K, Nassau J (1979). The history and present status of synthetic diamond. *Journal of Crystal Growth* 46(2):157-172.
- Nozaki H, Itoh S (1996). Structural stability of BC₂N. *Journal of Physics and Chemistry of Solids* 57:41-49.
- Perdew JP, Burke K, Ernzerhof M (1996). Generalized Gradient Approximation Made Simple *Physical Review Letters* 77:3865.
- Pugh SF (1954). Relations between the elastic moduli and the plastic properties of polycrystalline pure metals. *The London, Edinburgh, and Dublin Philosophical Magazine and Journal of Science* 45(367):823-843.
- Ranganathan SI, Ostojia-Starzewski M (2008). *Physical Review Letters*, The American Physical Society 101:055504.
- Reuss A, *Angew Z* (1929). Berechnung der Fließgrenze von Mischkristallen auf Grund der Plastizitätsbedingung für Einkristalle. *ZAMM—Journal of Applied Mathematics and Mechanics/Zeitschrift für Angewandte Mathematik und Mechanik* 9:49-58.
- Singh BP (1986). Characterization of cubic boron nitride compacts *Materials Research Bulletin* 21:85.
- Solozhenko VL, Andrault D, Fiquet G, Mezouar M, Rubie DC (2001). Synthesis of superhard cubic BC₂N. *Applied Physics Letters* 78:1385.
- Solozhenko VL, Gregoryanz E (2005). Synthesis of Superhard Materials. *Materials Today* 8:44.
- Stavrou E, Lobanov S, Dong H, Oganov AR, Prakapenka VB, Kon'opkov'a Z, Goncharov AF (2016). Synthesis of Ultra-incompressible sp³ Hybridized Carbon Nitride with 1:1 Stoichiometry. *Chemistry of Materials* 28:6925.
- Su C, Lv J, Li Q, Wang H, Zhang L, Wang Y, Ma Y (2017). Construction of crystal structure prototype database: Methods and Applications *Journal of Physics: Condensed Matter* 29:165901.
- Sun H, Jhi SH, Roundy D, Cohen ML, Louie SG (2001). Structural forms of cubic BC₂N. *Physical Review B*. 64(9):094108.
- Togo A, Tanaka I (2015). First principles phonon calculations in materials science *Scripta Materialia* 108:1-5.
- Voigt W (1928). *Lehrbuch der kristallphysik* (mit ausschluß der kristalloptik), edited by bg teubner and jw edwards, leipzig berlin. Ann Arbor, Mich.
- Wang Y, Lv J, Zhu L, Ma Y (2012). CALYPSO: A method for crystal structure prediction. *Computer Physics Communications* 183(10):2063-2070.
- Wang Y, Lv J, Li Q, Wang H, Ma Y (2019). *Handbook of Materials Modeling*, Springer International Publishing pp. 1-28.
- Zhao Y, He DW, Daemen LL, Shen TD, Schwarz RB, Zhu Y, Bish DL, Huang J, Zhang J, Shen G, Qian J, Zerda TW (2002). (Superhard B-C-N materials synthesized in nanostructured bulks *Journal of Materials Research* 17:3139.
- Zhao Z, Xu B, Tian Y (2016). Recent Advances in Superhard Materials *Annual Review of Materials Research* 46:383-406.